Pathway towards Programmable Wave Anisotropy in Cellular Metamaterials

Paolo Celli, Weiting Zhang, and Stefano Gonella

Phys. Rev. Applied **9**, 014014 — Published 12 January 2018

DOI: 10.1103/PhysRevApplied.9.014014

A pathway towards programmable wave anisotropy in cellular metamaterials

Paolo Celli,* Weiting Zhang, and Stefano Gonella†
Department of Civil, Environmental, and Geo- Engineering, University of Minnesota, Minneapolis, MN 55455, USA
(Dated: October 17, 2017)

In this work, we provide a proof-of-concept experimental demonstration of the wave control capabilities of cellular metamaterials endowed with populations of tunable electromechanical resonators. Each independently tunable resonator comprises a piezoelectric patch and a resistor-inductor shunt, and its resonant frequency can be seamlessly re-programmed without interfering with the cellular structure's default properties. We show that, by strategically placing the resonators in the lattice domain and by deliberately activating only selected subsets of them, chosen to conform to the directional features of the beamed wave response, it is possible to *override* the inherent wave anisotropy of the cellular medium. The outcome is the establishment of tunable spatial patterns of energy distillation resulting in a non-symmetric correction of the wavefields.

I. INTRODUCTION

Cellular solids are porous media known to display unique combinations of complementary mechanical properties, such as high stiffness and high strength at low densities [1]. *Lattice materials*—cellular solids with ordered architectures—are obtained by spatially tessellating a fundamental building block (unit cell) comprising simple slender structural elements such as beams, plates or shells. Advances in additive manufacturing have recently propelled a resurgence of architected cellular solids as mechanical metamaterials with unprecedented functionalities at multiple scales [2–5]. Examples include fully-recoverable, energy absorbing lattices with bucklable struts [6, 7], pentamode fluid-like materials that behave as "unfeelability" cloaks [8], lattices with negative Poisson's ratio [9], negative thermal expansion [10], and smart lattices with programmable stiffness [11].

Lattice structures also display unique dynamic properties. They commonly feature Bragg-type bandgaps as a result of their periodicity and occasionally subwavelength bandgaps for special unit cell designs or in the presence of internal resonators, thus behaving as frequency-selective stop-band filters for acoustic [12], elastic [13–19] and electromagnetic waves [20]. They also display elastic wave anisotropy, which manifests as pronounced beaming of the energy according to highly directional patterns [13, 21–30]. This behavior can be attributed to the fact that, at the cell scale, elastic waves are forced to propagate along the often tortuous pathways dictated by the links/struts. The spatial characteristics, symmetry landscape and frequency dependence of the anisotropic patterns are dictated by the unit cell's architecture [31, 32] and are usually irreversibly determined during the design and fabrication stages. To endow cellular solids with functional flexibility and active spatial wave management capabilities, we need our structural systems to be *tunable* or *programmable* [33–42]. To ensure that geometry and material requirements imposed by other functional constraints are preserved during the tuning process, it is especially important to devise minimally invasive tunability strategies [43].

In this work, we propose and implement a strategy for tailorable spatial wave management in architected cellular solids, based on the interplay between the inherent anisotropy of the underlying lattice medium and the resonant behavior of tunable resonators strategically located on selected lattice links. Let us recall here that a resonator attached to a structural medium interacts with an incident propagating wave by distilling from the wave spectrum an interval of frequencies comprised within the neighborhood of its resonant frequency [44, 45]. This behavior can be explained by invoking the destructive interference mechanisms between the incident wave and the wave that the resonator re-radiates, which experiences a 180° phase shift for frequencies immediately above resonance [46]. As a result, by tuning the resonators as to induce distillation at frequencies for which the lattice displays anisotropic directional wavefields, and by activating selected spatial subsets of resonators located along the dominant energy beams of the directional fields, we can override selected spatial wave features. The result is a smart lattice structure whose spatial wavefields can be programmed to display several *complementary* pattern corrections that *relax* the symmetry of the response. For this task, we resort to resonators consisting of thin, minimally invasive piezoelectric patches shunted with resistor-inductor (RL) circuits to realize resonant RLC units, adapting and perfecting a framework previously established for beams, plates and waveguides [45, 47–54]. The resonant frequency of each electromechanical resonator can be seamlessly varied by modifying the electrical impedance of the corresponding shunting circuit, which is carried out by simply tuning one of the circuit components.

* pcelli@umn.edu
† sgonella@umn.edu

II. EXPERIMENTAL SETUP

Our experimental setup is illustrated in Fig. 1a. The

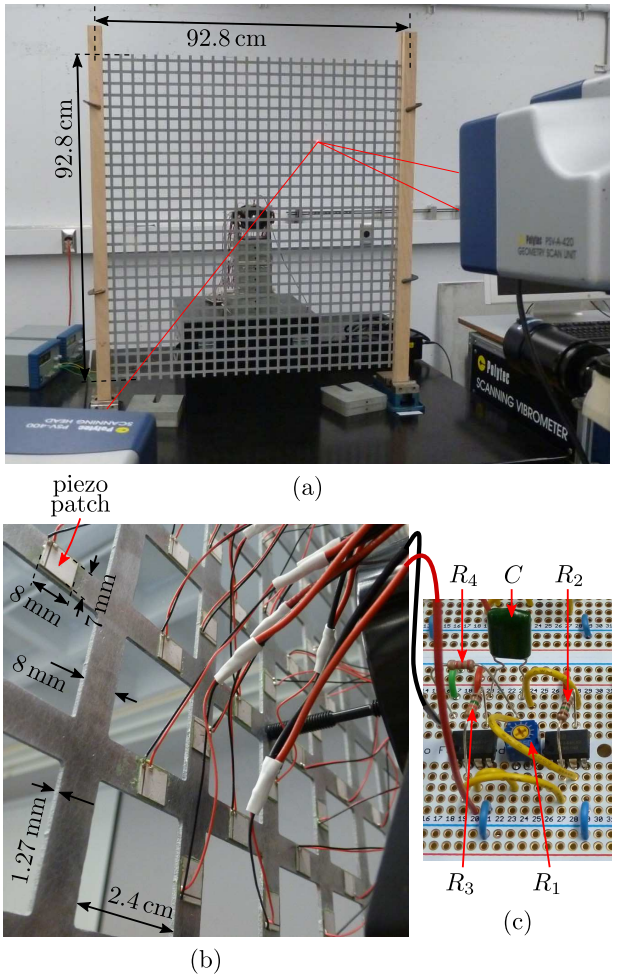

FIG. 1. (a) Experimental setup. (b) Detail of the rear face of the specimen near the actuation point, showing multiple piezoelectric patches bonded to the lattice structure. (c) One of the synthetic inductor circuits, schematically connected to one of the patches. Please consult the Supplemental Material [55] for details on the patch-circuit connection.

cellular medium of choice is a square lattice specimen, comprising 29×29 unit cells, manufactured out of a 1.27 mm-thick 6061 aluminum plate (Young's modulus $E = 68\,\text{GPa}$, density $\rho = 2700\,\text{kg/m}^3$, Poisson's ratio $\nu = 0.33$) using water jet cutting. The characteristic length of the unit cell is $L = 3.2\,\text{cm}$, and the width of a lattice link is $b = 8\,\text{mm}$. The out-of-plane motion of points on the front face of the specimen that correspond to a pre-determined scanning grid is measured via a 3D Scanning Laser Doppler Vibrometer (3D-SLDV). The excitation signals are imparted through an electromechanical shaker and a stinger, connected to the lattice node at the center of the specimen. A detail of the rear face of the specimen near the actuation location, shown in Fig. 1b, highlights the presence of multiple piezoelectric patches ($8 \times 7 \times 0.2\,\text{mm}$ wafers made of PZT-5A) bonded to the structure. A total of 28 patches are located as to form a ring around the excitation point. All the patches are wired, but only up to seven (or eight) are simultaneously activated—i.e. connected to a RL circuit—during each experiment. Eight synthetic inductors (Antoniou circuits) are built on a solderable breadboard to serve as equivalent inductors for the eight required shunting circuits; one of them is shown in Fig. 2c. Synthetic inductors are a staple in the shunting literature due to their compact dimensions (even for large values of inductance), versatility and tunability [56]. DC power supplies are used to power the Op-Amps in the Antoniou circuits. To seamlessly program the synthetic inductor (and consequently the characteristics of the resonator), the resistor R_1 in each circuit is a tunable potentiometer; modifying R_1 changes the equivalent inductance $L_{eq} = R_1R_3R_4C/R_2$ and, therefore, the resonant frequency $f_r = 1/[2\pi(C^pL_{eq})^{1/2}]$, where C^p is the capacitance of the piezo patch. The circuit components are selected as to allow the resonators to be tuned at any frequency in the interval from 2 to 13 kHz. Series resistors are required to introduce enough damping to alleviate the effects of circuit instabilities [57]. More details on the experimental setup, on the circuits and on their tuning are reported in the Supplemental Material [55].

III. NUMERICAL AND EXPERIMENTAL WAVE RESPONSE

The default wave response of the pristine lattice is illustrated in Fig. 2. The band diagram of an infinite lattice having the same cell dimensions, geometry and material properties as our specimen is shown in Fig. 2a; this result is obtained through a Bloch analysis of a unit cell modeled with plate finite elements (implementing Mindlin's plate model) limited to wave vectors sampled along the contour of the Irreducible Brillouin Zone (IBZ) [13]. We are especially interested in frequencies where the appearance of partial bandgaps suggests pronounced wave anisotropy. In the low-frequency range shown in Fig. 2a, these frequencies are approximately 2.35 kHz and 4.1 kHz. The blue lines in Fig. 2b mark the Cartesian iso-frequency contour obtained by slicing the first dispersion surface at 2.35 kHz, and highlight how, at this frequency, waves are predominantly allowed to propagate along directions that are $\pm45^\text{o}$-oriented with respect to the horizontal axis. Iso-frequency contours provide information analogous to the slowness curves [58], whereby proximity to the origin implies high phase velocity, and vice versa. The iso-frequency contour of the second surface at 4.1 kHz displays complementary features: wave speeds are now much higher along the horizontal and vertical directions.

In Fig. 3, we report the out-of-plane velocity snapshots (at two time instants) of the measured transient

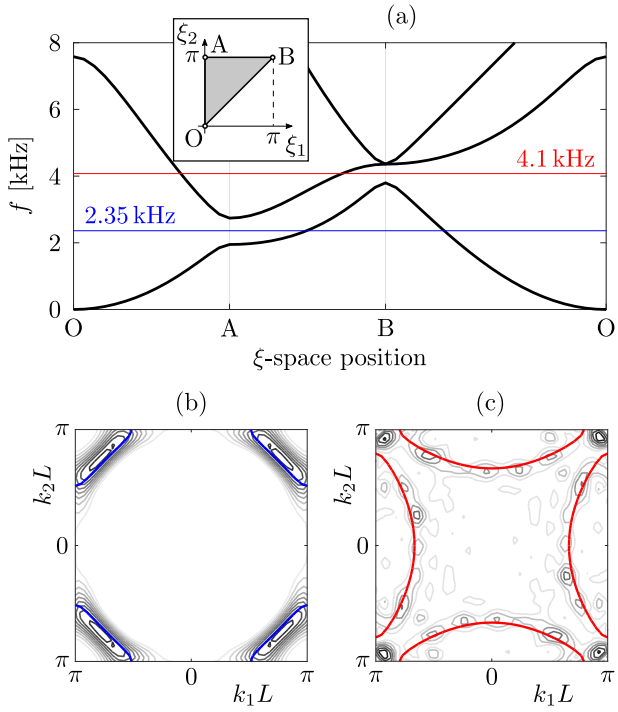

FIG. 2. (a) Band diagram of the pristine square lattice computed via a FE-based unit cell analysis. This diagram only comprises flexural wave modes, i.e., those relevant in the case of low-frequency, out-of-plane loads. The Irreducible Brillouin zone is shown in the insert. Colored horizontal lines highlight frequencies where wave anisotropy is most pronounced. (b) The blue lines represent the numerically computed iso-frequency contour of the first dispersion surface at 2.35 kHz; the underlying contours are the spectral lines computed from the experimental lattice response to a burst with carrier frequency 2.35 kHz. (c) Same as (b) for the second dispersion surface at 4.1 kHz.

response of our lattice specimen. The excitation signals are 13-cycle bursts with carrier frequencies corresponding to 2.35 kHz and 4.1 kHz, respectively. Note that, at this stage, all patches are in their open circuit configuration. The response at 2.35 kHz (Fig. 3a) shows that, at this frequency, the wavefields feature four highly-beamed packets propagating along ±45°-oriented directions, as predicted by the iso-frequency contour in Fig. 2b. On the other hand, the wavefields corresponding to 4.1 kHz (Fig. 3b) feature packets propagating mainly along the vertical and horizontal directions—consistent with the predictions of Fig. 2c. In Figs. 2b-c, to further demonstrate the excellent agreement between the results from the unit cell analysis and the laser-acquired experimental data, we superimpose to the iso-frequency contours the spectral lines of the lattice response at the same frequencies, obtained from the experimentally acquired wavefields through a 2D Discrete Fourier Transform procedure (2D-DFT; see the SM section for details on the reconstruction procedure). This comparison also highlights how the presence of the open circuit (non-shunted)

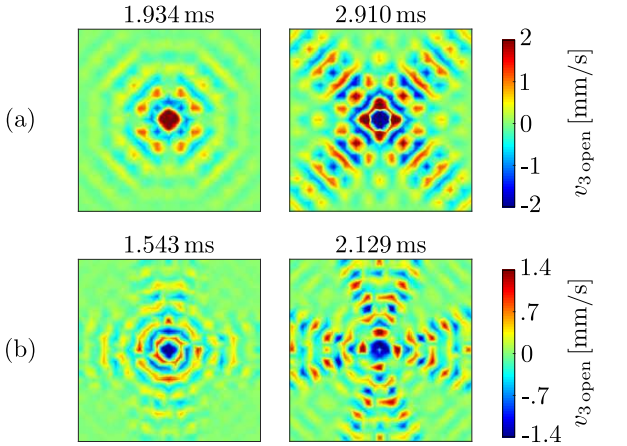

FIG. 3. Transient experimental response of the lattice to 13-cycle bursts with carrier frequencies (a) 2.35 kHz and (b) 4.1 kHz, when all piezoelectric patches are in their open circuit configuration.

patches has minimal influence on the characteristics of the medium in this low-frequency regime.

IV. WAVE-RESONATOR INTERACTION

To elucidate the mechanisms behind the wave-resonator interaction in the specific case where the resonator comprises a piezoelectric patch shunted with a RL circuit, we resort to a simple one dimensional experiment. The specimen is a 117.4 cm-long and 8 mm-wide beam with the same thickness and material properties as the lattice specimen. The beam is clamped at both ends, and the excitation is imparted near one of the clamps. Approximately at the center of the beam, we bond a single piezoelectric patch (identical to those used in the lattice experiment). A schematic of the beam, with illustration of the location where the response is measured by the 3D-SLDV system, is shown in Fig. 4a (the setup for this experiment is shown in Fig. S7 and discussed in the Supplemental Material [55]). The beam is excited via a 9-cycle burst with carrier frequency 3.5 kHz. Boundary reflections are eliminated through a time-filtering procedure, also discussed in [55]. In Fig. 4b, we compare the frequency spectra of the out-of-plane velocity signals recorded in the open circuit case (gray line) and in the shunted case (black line). These signals have been obtained by averaging the response at multiple measurement points located after the resonator. The patch-circuit system is tuned as to resonate around 3.5 kHz, although a small error in pinpointing the frequency is often expected. We observe that, as predicted, the resonator causes wave attenuation/distillation in the neighborhood of the tuning frequency. The amplitude of attenuation is small compared to other instances reported in the literature on shunted systems due to the fact that here the wave packet is purely incident and interacts with the

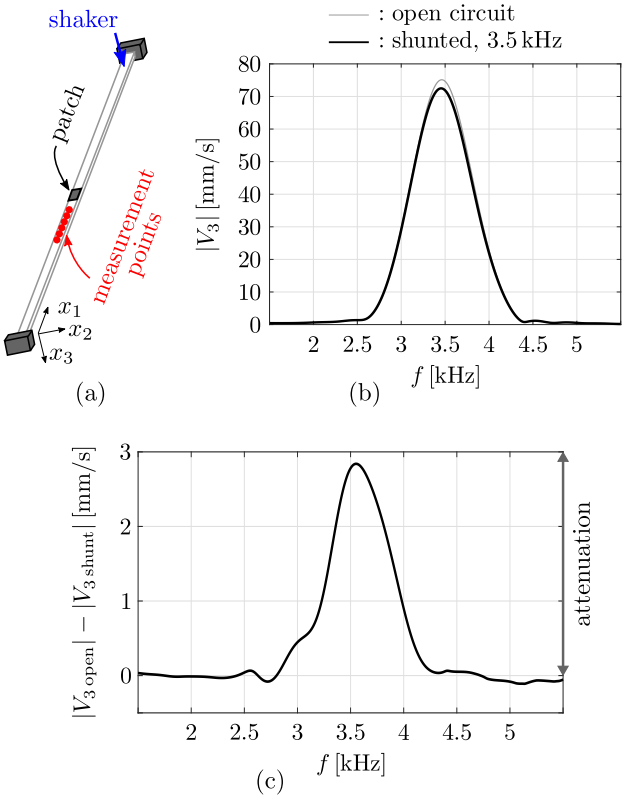

FIG. 4. Experimental results on wave-resonator interaction. (a) Schematic of the experimental setup (clamped-clamped beam with a single piezoelectric patch). (b) Frequency spectra of the filtered out-of-plane velocity time histories for open-circuit and shunted cases, in response to a burst with 3.5 kHz carrier frequency. The curves are obtained by averaging the spectra recorded at multiple measurement points downstream from the patch. (c) Difference between the open circuit spectrum and the shunted one.

resonator only once. Stronger attenuation results usually arise from multiple wave-resonator interactions, as in steady-state conditions or when we can aggregate the effects of multiple transient packets bouncing back and forth between the structure's boundaries [45]. The action of the resonator can be better visualized by subtracting the shunted spectrum from the open circuit one; this differential plot is shown in Fig. 4c. Notably, most of the attenuation is recorded right above the expected resonance. This behavior can be qualitatively explained using arguments of phase delay and wave interference. Specifically, when a propagating wave interacts with a resonator, a fraction of the energy is stored in the resonator and re-radiated into the structure, possibly with a phase shift. This wave can interact constructively or destructively with the incident wave, according to their relative phase [44, 46, 59]; above resonance, where incident and re-radiated wave are in opposition of phase, destructive interference mechanisms result in signal attenuation. This effect becomes less pronounced as we move away from resonance, the resonator becomes progressively less engaged and the portion of the reradiated energy drops, ultimately dictating the width of the bandgap. Note that, while this effect is precisely observed for continuous harmonic excitation (which explains why the onset of resonant bandgaps in the frequency domain can be pinpointed experimentally with great accuracy in steady state conditions), its signature is blurrier for burst excitations with compact support where issues of packet delay and distortion may contaminate the inference.

V. ANISOTROPY OVERRIDING

At this stage, we know how the lattice responds to bursts at several frequencies of interest and how a traveling wave interacts with an electromechanical resonator based on a shunted piezo patch. Therefore, we have all the ingredients to investigate the influence of strategically placed, properly tuned resonators on specific wave features of the anisotropic response of the lattice. A numerical demonstration of this strategy for an idealized lattice of springs and masses with mass-in-mass nodes, which can be seen as a purely mechanical analog of our system, is reported in the Supplemental Material [55]. Despite the pronounced modeling differences, these simulations are insightful in that they allow to freely explore the parameter space of the population of resonators far beyond the constraints of the experiments. Back to our experiments, we first consider the lattice response at 2.35 kHz, shown in Fig. 3a. Our goal is to override one of the four $\pm 45^{\circ}$-oriented packets propagating from the excitation point. In our first test, we shunt eight patches located along the path of the packet propagating towards the bottom-left corner of the domain. The selected patches, located on the links highlighted by cross-shaped markers in Fig. 5a, are connected to the synthetic inductors on the circuit board through series resistors with resistance $R_s = 1\,\mathrm{k}\Omega$. Each resonator is tuned at 2.2 kHz (see the Supplemental Material for details on the tuning procedure [55]); we choose this lower tuning frequency rather than the nominal 2.35 kHz to compensate for the shift in resonance caused by the large value of R_s (necessary to avoid circuit instabilities). The response of the lattice at three distinct time instants is shown in the top row of Fig. 5b. At first glance, we do not detect any macroscopic modification with respect to the open circuit response of Fig. 3a. To further explore the data and reveal potential higher-order correction effects in the shunted response, in the bottom row of Fig. 5b, we report the differential wavefields obtained by subtracting the shunted response from the open circuit one at the considered time instants. Upon this operation, an asymmetric pattern consistent with our expectations unfolds. As predicted, properly-tuning a selected subset of resonators produces a frequency-distillation (and consequently an amplitude correction) of the wave packet in the spatial neighborhood of the activated resonators: packets traveling from the source towards the bottom-left corner of the domain

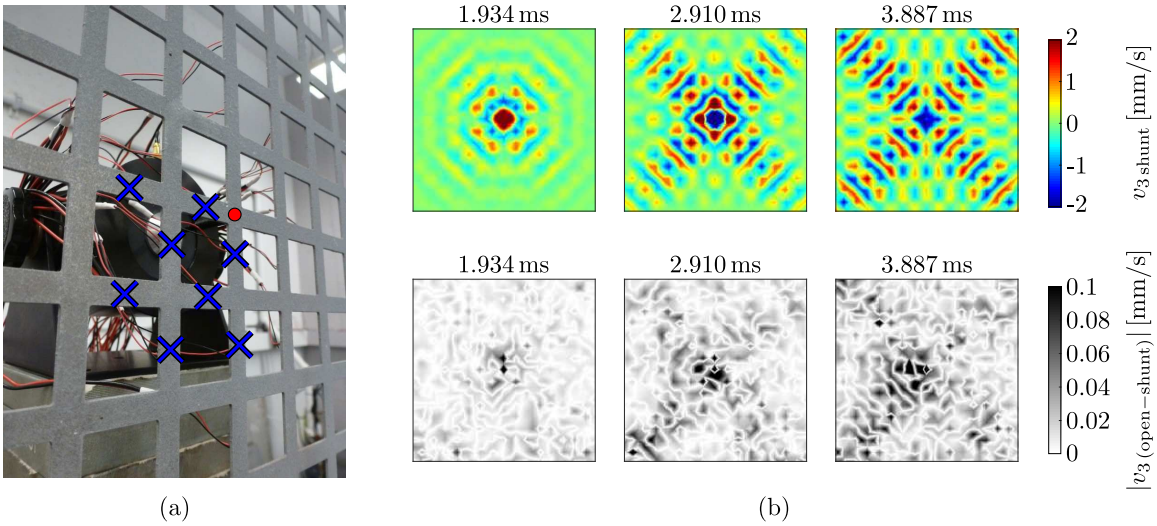

FIG. 5. Anisotropy overriding at 2.35 kHz; the targeted wave feature is the packet propagating towards the bottom-left corner of the specimen. (a) Detail of the front (scanned) face of the specimen; the circular marker indicates the actuation location and the crosses denote the links with shunted piezos. (b) Top row: wavefields acquired at three time instants. Bottom row: spatial patterns displayed by the difference between the open circuit and the shunted response.

carry the strongest signature of shunting. In Fig. 6, we report the velocity time histories recorded at four characteristic locations on the specimen's surface—one point in each quadrant of the scanned area (top-right, bottom-right, bottom-left and top-left). These results confirm that waves propagating towards the bottom-left corner are the most affected by the resonators and indeed experience wave attenuation. These and other results in this Section, albeit representing an unequivocal proof of concept of the anisotropy overriding capabilities of shunted lattices, reflect effects that are one order of magnitude smaller than the amplitude of the wave response. Stronger attenuation results could ostensibly be attainable through refinements of the experimental setup, e.g., by using a larger number of simultaneously activated resonators or by working with improved circuitry with reduced parasitic resistance. These technological improvements will be addressed in future investigations.

To demonstrate the tunability of our metamaterial system, we re-program the lattice by shunting a different set of patches and re-tuning the circuits as to override the wave packet propagating, still at 2.35 kHz, towards the top-left corner of the domain. Note that re-tuning is needed since each patch has a slightly different capacitance. This experiment is illustrated in Fig. 7. In this second scenario, we again manage to override the desired feature of the anisotropic wave pattern.

We now shift our attention towards the wave response at 4.1 kHz—characterized by complementary wave patterns propagating along the vertical and horizontal directions as illustrated in Fig. 3b. By shunting seven patches located on the links immediately to the right of the excitation point as indicated in Fig. 8a, we program the system to override the right-going wave packet. Note

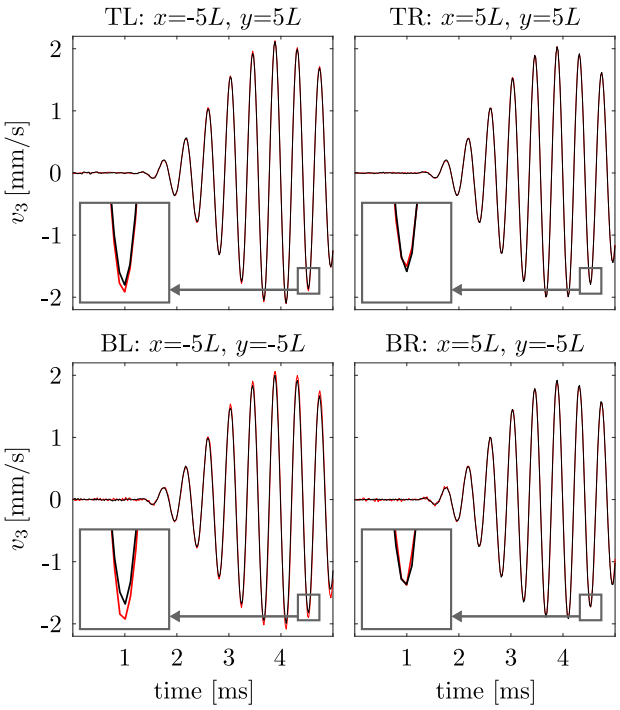

FIG. 6. Clockwise: time histories of the open circuit (red line) and shunted (black line) response at four points in the top-left (TL), top-right (TR), bottom-left (BL) and bottom-right (BR) quadrants, respectively. The targeted wave feature is the packet propagating towards the bottom-left corner of the specimen.

that, in this case, the resonators are tuned exactly at 4.1 kHz, since the required 330 Ω series resistance seems not to produce any appreciable shift in resonance fre-

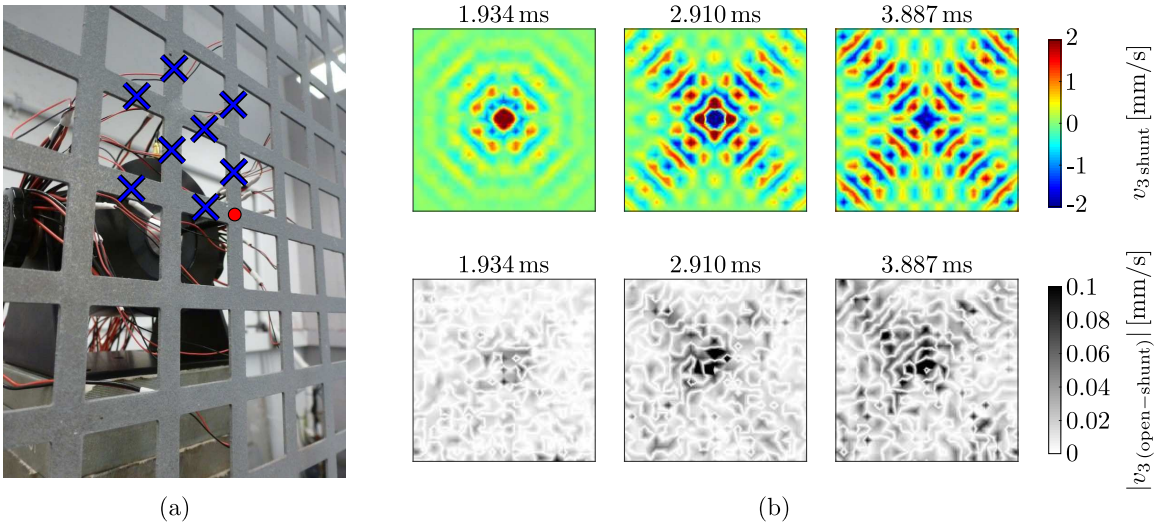

(a) (b)

FIG. 7. Anisotropy overriding at 2.35 kHz; the targeted wave feature is the packet propagating towards the top-left corner of the specimen. (a) Detail of the front (scanned) face of the specimen, indicating where the shunted patches are located. (b) Top row: wavefields acquired at three time instants. Bottom row: spatial patterns displayed by the difference between the open circuit and the shunted response.

quency. The differential wavefields in Fig. 8b show that the right-going horizontal feature is indeed the one being attenuated by the resonators. An additional result targeting another direction of propagation is reported for completeness in the Supplemental Material.

VI. CONCLUSIONS

In this work, we have demonstrated that the frequency-selective anisotropic wave patterns intrinsically established in cellular metamaterials can be corrected by resorting to clouds of strategically placed, tunable electromechanical resonators and by selecting objective-specific spatial activation strategies. We have shown that we can achieve levels of programmability that allow to override the anisotropy of the wave response along different directions and at different frequencies. It is reasonable to assume that results similar to those shown in this proof-of-concept study for a simple square lattice would be achievable in more complex two- and three-dimensional architected cellular solids, albeit requiring even more complex electromechanical control systems. Integrated manufacturing of the electromechanical resonators, improved circuitry [60], or the adoption of less invasive resonators capable of offering a stronger coupling while simultaneously allowing the activation of more than seven or eight resonators could increase the tangibility of the observed effects. This kind of developments will eventually pave the way towards families of smart lattices with programmable spatial wave control capabilities such as wave steering, energy channeling and re-routing, and spatial filtering.

ACKNOWLEDGMENTS

We acknowledge the support of the National Science Foundation (grant CMMI-1266089). PC acknowledges the support of the University of Minnesota through the Doctoral Dissertation Fellowship. We also thank Davide Cardella for his contribution during the initial stages of the project.

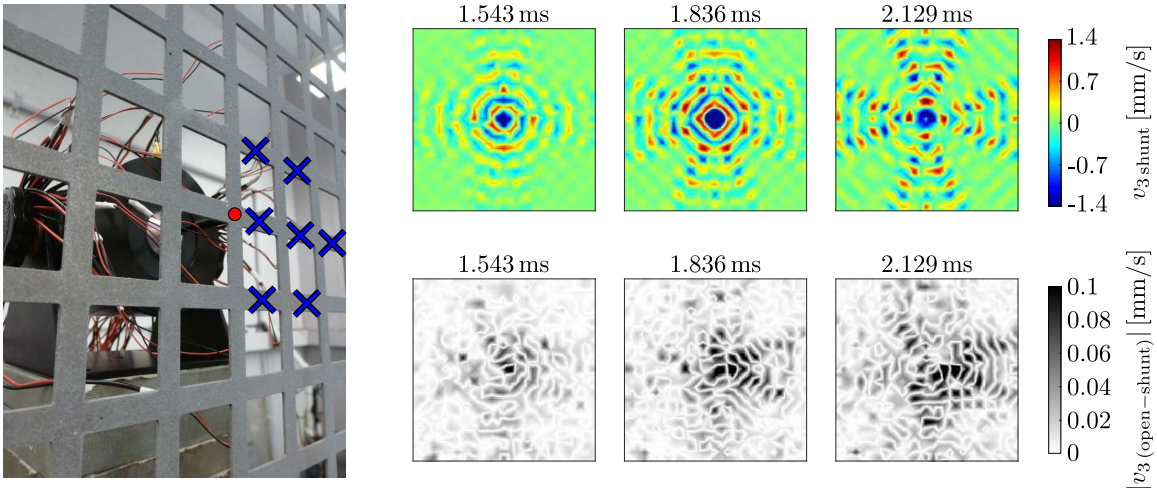

(a) (b)

FIG. 8. Anisotropy overriding at 4.1 kHz; the targeted wave feature is the rightward-propagating packet. (a) Detail of the front (scanned) face of the specimen, indicating where the shunted patches are located. (b) Top row: wavefields acquired at three time instants. Bottom row: spatial patterns displayed by the difference between the open circuit and the shunted response.

[1] N. A. Fleck, V. S. Deshpande, and M. F. Ashby, "Micro-architectured materials: past, present and future," Proc. R. Soc. A **466**, 2495–2516 (2010).

[2] T. A. Schaedler, A. J. Jacobsen, A. Torrents, A. E. Sorensen, J. Lian, J. R. Greer, L. Valdevit, and W. B. Carter, "Ultralight metallic microlattices," Science **334**, 962–965 (2011).

[3] X. Zheng, H. Lee, T. H. Weisgraber, M. Shusteff, J. DeOtte, E. B. Duoss, J. D. Kuntz, M. M. Biener, Q. Ge, J. A. Jackson, S. O. Kucheyev, N. X. Fang, and C. M. Spadaccini, "Ultralight, ultrastiff mechanical metamaterials," Science **344**, 1373–1377 (2014).

[4] L. R. Meza, A. J. Zelhofer, N. Clarke, A. J. Mateos, D. M. Kochmann, and J. R. Greer, "Resilient 3d hierarchical architected metamaterials," Proc. Natl. Acad. Sci. U.S.A. **112**, 11502–11507 (2015).

[5] C. Coulais, E. Teomy, K. de Reus, Y. Shokef, and M. van Hecke, "Combinatorial design of textured mechanical metamaterials," Nature **535**, 529–532 (2016).

[6] S. Shan, S. H. Kang, J. R. Raney, P. Wang, L. Fang, F. Candido, J. A. Lewis, and K. Bertoldi, "Multistable architected materials for trapping elastic strain energy," Adv. Mater. **27**, 4296–4301 (2015).

[7] D. Restrepo, N. D. Mankame, and P. D. Zavattieri, "Phase transforming cellular materials," Extreme Mech. Lett. **4**, 52–60 (2015).

[8] T. Bückmann, M. Thiel, M. Kadic, R. Schittny, and M. Wegener, "An elasto-mechanical unfeelability cloak made of pentamode metamaterials," Nat. Commun. **5**, 4130 (2014).

[9] R. Lakes, "Advances in negative poisson's ratio materials," Adv. Mater. **5**, 293–296 (1993).

[10] Q. Wang, J. A. Jackson, Q. Ge, J. B. Hopkins, C. M. Spadaccini, and N. X. Fang, "Lightweight mechanical metamaterials with tunable negative thermal expansion," Phys. Rev. Lett. **117**, 175901 (2016).

[11] Y. Song, P. C. Dohm, B. Haghpanah, A. Vaziri, and J. B. Hopkins, "An active microarchitectured material that utilizes piezo actuators to achieve programmable properties," Adv. Eng. Mater. **18**, 1113–1117 (2016).

[12] S. Krödel and C. Daraio, "Microlattice metamaterials for tailoring ultrasonic transmission with elastoacoustic hybridization," Phys. Rev. Applied **6**, 064005 (2016).

[13] A. S. Phani, J. Woodhouse, and N. A. Fleck, "Wave propagation in two-dimensional periodic lattices," J. Acoust. Soc. Am. **119**, 1995–2005 (2006).

[14] E. Baravelli and M. Ruzzene, "Internally resonating lattices for bandgap generation and low-frequency vibration control," J. Sound Vib. **332**, 6562–6579 (2013).

[15] S. Krödel, T. Delpero, A. Bergamini, P. Ermanni, and D. M. Kochmann, "3d auxetic microlattices with independently controllable acoustic band gaps and quasi-static elastic moduli," Adv. Eng. Mater. **16**, 357–363 (2014).

[16] L. Junyi and D.S. Balint, "A parametric study of the mechanical and dispersion properties of cubic lattice structures," Int. J. Solids Struct. **91**, 55–71 (2016).

[17] M. Miniaci, A. Krushynska, A. B. Movchan, F. Bosia, and N. M. Pugno, "Spider web-inspired acoustic metamaterials," Appl. Phys. Lett. **109**, 071905 (2016).

[18] K. H. Matlack, A. Bauhofer, S. Krödel, A. Palermo, and C. Daraio, "Composite 3d-printed metastructures for low-frequency and broadband vibration absorption," Proc. Natl. Acad. Sci. U.S.A. **113**, 8386–8390 (2016).

[19] F. Warmuth, M. Wormser, and C. Körner, "Single phase 3d phononic band gap material," Sci. Rep. **7**, 3843 (2017).

[20] V. F. Chernow, H. Alaeian, J. A. Dionne, and J. R. Greer, "Polymer lattices as mechanically tunable 3-dimensional photonic crystals operating in the infrared," Appl. Phys. Lett. **107**, 101905 (2015).

[21] R. S. Langley, "The response of two-dimensional periodic structures to point harmonic forcing," J. Sound. Vib. **197**, 447–469 (1996).

[22] M. Ruzzene, F. Scarpa, and F. Soranna, "Wave beaming effects in two-dimensional cellular structures," Smart Mater. Struct. **12**, 363 (2003).

[23] J. Wen, D. Yu, G. Wang, and X. Wen, "Directional propagation characteristics of flexural wave in two-dimensional periodic grid-like structures," J. Phys. D: Appl. Phys. **41**, 135505 (2008).

[24] G. Carta, M. Brun, A.B. Movchan, N.V. Movchan, and I.S. Jones, "Dispersion properties of vortex-type monatomic lattices," Int. J. Solids Struct. **51**, 2213–2225 (2014).

[25] P. Celli and S. Gonella, "Laser-enabled experimental wavefield reconstruction in two-dimensional phononic crystals," J. Sound. Vib. **333**, 114–123 (2014).

[26] Y-F. Wang, Y-S. Wang, and C. Zhang, "Bandgaps and directional propagation of elastic waves in 2d square zigzag lattice structures," J. Phys. D: Appl. Phys. **47**, 485102 (2014).

[27] G. Trainiti, J.J. Rimoli, and M. Ruzzene, "Wave propagation in undulated structural lattices," Int. J. Solids Struct. **97**, 431–444 (2016).

[28] A. J. Zelhofer and D. M. Kochmann, "On acoustic wave beaming in two-dimensional structural lattices," Int. J. Solids Struct. **115-116**, 248–269 (2017).

[29] R. Ganesh and S. Gonella, "Experimental evidence of directivity-enhancing mechanisms in nonlinear lattices," Appl. Phys. Lett. **110**, 084101 (2017).

[30] G. Lefebvre, T. Antonakakis, Y. Achaoui, R. V. Craster, S. Guenneau, and P. Sebbah, "Unveiling extreme anisotropy in elastic structured media," Phys. Rev. Lett. **118**, 254302 (2017).

[31] P. Celli and S. Gonella, "Low-frequency spatial wave manipulation via phononic crystals with relaxed cell symmetry," J. Appl. Phys. **115**, 103502 (2014).

[32] D. Krattiger, R. Khajehtourian, C. L. Bacquet, and M. I. Hussein, "Anisotropic dissipation in lattice metamaterials," AIP Adv. **6**, 121802 (2016).

[33] M. Ruzzene and A. Baz, "Control of wave propagation in periodic composite rods using shape memory inserts," J. Vib. Acoust. **122**, 151–159 (2000).

[34] S. Shan, S. H. Kang, P. Wang, C. Qu, S. Shian, E. R. Chen, and K. Bertoldi, "Harnessing multiple folding mechanisms in soft periodic structures for tunable control of elastic waves," Adv. Funct. Mater. **24**, 4935–4942 (2014).

[35] M. A. Nouh, O. J. Aldraihem, and A. Baz, "Periodic metamaterial plates

with smart tunable local resonators," J. Intell. Mater. Syst. Struct. **27**, 1829–1845 (2016).
[36] R. Zhu, Y. Y. Chen, M. V. Barnhart, G. K. Hu, C. T. Sun, and G. L. Huang, "Experimental study of an adaptive elastic metamaterial controlled by electric circuits," Appl. Phys. Lett. **108**, 011905 (2016).
[37] R. Zhu, Y. Y. Chen, Y. S. Wang, G. K. Hu, and G. L. Huang, "A single-phase elastic hyperbolic metamaterial with anisotropic mass density," J. Acoust. Soc. Am. **139**, 3303–3310 (2016).
[38] C. Croënne, M. Ponge, B. Dubus, C. Granger, L. Haumesser, F. Levassort, J. O. Vasseur, A. Lordereau, M. P. Thi, and A. C. Hladky-Hennion, "Tunable phononic crystals based on piezoelectric composites with 1-3 connectivity," J. Acoust. Soc. Am. **139**, 3296–3302 (2016).
[39] Z. Wang, Q. Zhang, K. Zhang, and G. K. Hu, "Tunable digital metamaterial for broadband vibration isolation at low frequency," Adv. Mater. **28**, 9857–9861 (2016).
[40] M. Ouisse, M. Collet, and F. Scarpa, "A piezo-shunted kirigami auxetic lattice for adaptive elastic wave filtering," Smart Mater. Struct. **25**, 115016 (2016).
[41] Y. Chen, T. Li, F. Scarpa, and L. Wang, "Lattice metamaterials with mechanically tunable poisson's ratio for vibration control," Phys. Rev. Applied **7**, 024012 (2017).
[42] O. R. Bilal, A. Foehr, and C. Daraio, "Reprogrammable phononic metasurfaces," Adv. Mater. , 1700628 (2017).
[43] P. Celli and S. Gonella, "Tunable directivity in metamaterials with reconfigurable cell symmetry," Appl. Phys. Lett. **106**, 091905 (2015).
[44] Z. Liu, X. Zhang, Y. Mao, Y. Y. Zhu, Z. Yang, C. T. Chan, and P. Sheng, "Locally resonant sonic materials," Science **289**, 1734–1736 (2000).
[45] D. Cardella, P. Celli, and S. Gonella, "Manipulating waves by distilling frequencies: a tunable shunt-enabled rainbow trap," Smart Mater. Struct. **25**, 085017 (2016).
[46] F. Lemoult, N. Kaina, M. Fink, and G. Lerosey, "Wave propagation control at the deep subwavelength scale in metamaterials," Nat. Phys. **9**, 55–60 (2013).
[47] N. W. Hagood and A. von Flotow, "Damping of structural vibrations with piezoelectric materials and passive electrical networks," J. Sound Vib. **146**, 243–268 (1991).
[48] F. Casadei, M. Ruzzene, L. Dozio, and K. A. Cunefare, "Broadband vibration control through periodic arrays of resonant shunts: experimental investigation on plates," Smart Mater. Struct. **19**, 015002 (2010).
[49] L. Airoldi and M. Ruzzene, "Design of tunable acoustic metamaterials through periodic arrays of resonant shunted piezos," New J. Phys. **13**, 113010 (2011).
[50] F. Casadei, T. Delpero, A. Bergamini, P. Ermanni, and M. Ruzzene, "Piezoelectric resonator arrays for tunable acoustic waveguides and metamaterials," J. Appl. Phys. **112**, 064902 (2012).
[51] A. Bergamini, T. Delpero, L. De Simoni, L. De Lillo, M. Ruzzene, and P. Ermanni, "Phononic crystal with adaptive connectivity," Adv. Mater. **26**, 1343–1347 (2014).
[52] J. Wen, S. Chen, G. Wang, D. Yu, and X. Wen, "Directionality of wave propagation and attenuation in plates with resonant shunting arrays," J. Intell. Mater. Syst. Struct. **27**, 28–38 (2016).
[53] C. Sugino, S. Leadenham, M. Ruzzene, and A. Erturk, "An investigation of electroelastic bandgap formation in locally resonant piezoelectric metastructures," Smart Mater. Struct. **26**, 055029 (2017).
[54] M. Collet, M. Ouisse, and F. Tateo, "Adaptive metacomposites for vibroacoustic control applications," IEEE Sens. J. **96**, 2145–2152 (2014).
[55] See Supplemental Material (in tail of this document) for a more detailed account on the experimental setups and for additional results. It includes Ref. [61, 62].
[56] G. Wang, S. Chen, and J. Wen, "Low-frequency locally resonant band gaps induced by arrays of resonant shunts with antoniou's circuit: experimental investigation on beams," Smart Mater. Struct. **20**, 015026 (2011).
[57] F. dell'Isola, C. Maurini, and M. Porfiri, "Passive damping of beam vibrations through distributed electric networks and piezoelectric transducers: prototype design and experimental validation," Smart Mater. Struct. **13**, 299 (2004).
[58] D. Tallarico, N. V. Movchan, A. B. Movchan, and D. J. Colquitt, "Tilted resonators in a triangular elastic lattice: Chirality, bloch waves and negative refraction," J. Mech. Phys. Solids **103**, 236–256 (2017).
[59] Y. Jin, B. Bonello, R. P. Moiseyenko, Y. Pennec, O. Boyko, and B. Djafari-Rouhani, "Pillar-type acoustic metasurface," Phys. Rev. B **96**, 104311 (2017).
[60] E. A. Flores Parra, A. Bergamini, L. Kamm, P. Zbinden, and P. Ermanni, "Implementation of integrated 1d hybrid phononic crystal through miniaturized programmable virtual inductances," Smart Mater. Struct. **26**, 067001 (2017).
[61] F. A. C. Viana and V. Steffen Jr, "Multimodal vibration damping through piezoelectric patches and optimal resonant shunt circuits," J. Braz. Soc. Mech. Sci. Eng. **28**, 293–310 (2006).
[62] H. H. Huang, C. T. Sun, and G. L. Huang, "On the negative effective mass density in acoustic metamaterials," Int. J. Eng. Sci. **47**, 610–617 (2009).